Journal of Oceanography, Vol. 58, pp. 651 to 660, 2002

Behavior of Warm-Core Rings in a Double-Gyre Wind-Driven Ocean Circulation Model

SACHIHIKO ITOH* and TAKASHIGE SUGIMOTO

Ocean Research Institute, University of Tokyo, Minamidai, Nakano-ku, Tokyo 164-8639, Japan

(Received 15 November 2001; in revised form 15 March 2002; accepted 16 March 2002)

Numerical experiments have been performed to understand the movement of warm-core rings in the Kuroshio-Oyashio Transition region, considering the double-gyre ocean circulation represented by a 2.5-layer primitive equation model. Rings, eddies, and frontal disturbances are simulated, and analytical descriptions of warm-core ring behavior are examined. Warm-core rings are usually generated at the south of the zero wind stress curl line (ZWCL), either off-shore or near-shore, and a near-shore ring gradually moves northward along the coast, supplied with energy from the subtropical front and other rings. When they approach the ZWCL, two different types of movements occur, which is affected by the intensity of the rings and controlled by the wind stresses. In case the ring intensity is strong, it moves northward along the coast against the subarctic western boundary current system and cold-core rings, whereas a moderate ring is advected by them to the northeastward. The advection process of moderate rings seems to be important for northeastward movement of the Kuroshio warm-core rings in the middle of the Oyashio current system. The mechanism of large-scale forcing dynamics influences the cross-shore location of rings and implications for the fishing ground formation of the Pacific saury are described.

Keywords:
· Double-gyre wind-driven ocean circulation model,
· warm-core rings,
· Kuroshio-Oyashio Transition region.

1. Introduction

Large, intense warm-core rings are often observed in the Kuroshio-Oyashio Transition region. They are baroclinic anticyclones with a diameter of about 200 km and a thickness extending over 1000 m. The core water has its origin in the Kuroshio, which is warm, saline, and nutrient poor compared to the Oyashio or mixed water of both areas. Warm-core rings sometimes stay for several years in the Kuroshio-Oyashio Transition region (hereafter referred as KOTR) gradually moving northward (Fig. 1(a)), which is unique compared to other warm-core rings such as Gulf Stream rings. Itoh and Sugimoto (2001b) showed that a warm-core ring could move northward interacting with a steep slope (Fig. 1(b)), but the interaction of a ring and the Kuroshio, Oyashio, and other rings are not considered in their experiments. Warm-core rings initially located off-shore, east of the continental slope, were observed to move westward (Mizuno and White, 1983), some of them merging with other rings around the continental slope and consequently supplying heat and mechanical energy to them (Yasuda *et al*., 1992). Itoh and Sugimoto (2001a) reported that the movement of the warm-core ring 93A, the recent representative of a long-lived ring, were synchronized with the seasonal variation of the volume transport of the Oyashio besides the northward alongshore tendency: it moved southward in winter when the transport is large.

Some studies stated that eddies play an important role in the vorticity budget of double-gyre ocean circulation with asymmetrical wind forcing (Verron and Provost, 1991; Yasuda and Hanawa, 1996). The meridional movement of an eddy away from one gyre results in the transportation of the vorticity of their own to the other gyre, and the ensemble of the effect, i.e. the summation of the effect of all eddies, was shown to be significant in those studies. It is thus expected that the general behavior of the warm-core rings that consists of the individual physical processes can be explained by large-scale ocean circulation. Note that we use the word "warm-core ring" or simply "ring" as a distinct anticyclonic vortex in contrast to the word "eddy" which generally includes "ring" in the broad sense. In this study the double-gyre wind-driven circulation is numerically modeled, and the behavior of the warm-core rings is examined.

* Corresponding author. E-mail: itohsach@ori.u-tokyo.ac.jp

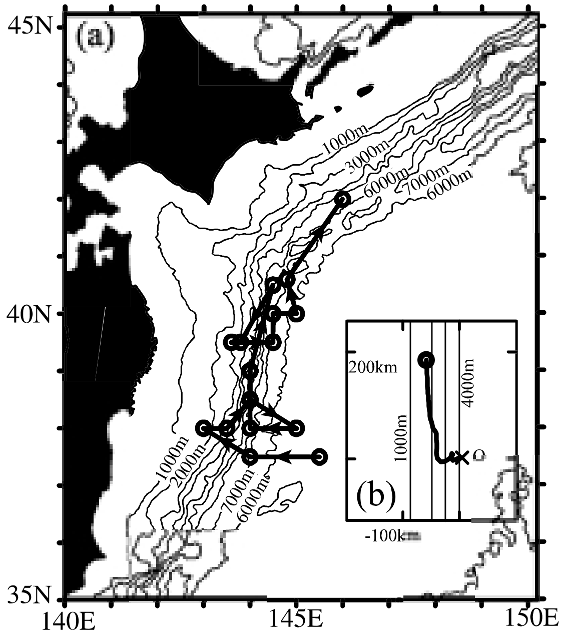

Fig. 1. (a) Trajectory of the warm-core ring 93A observed from February 1993 to November 1997: the time interval of the plot is three months. (b) Trajectory of a model warm-core ring for 200 days calculation in Itoh and Sugimoto (2001b) with the same spatial scale as (a).

Table 1. Model parameters.

Layer thickness	$H_1 = 500$, $H_2 = 1500$ [m]
Coriolis parameter	$f = 0.33$–1.2 [10^{-4}s^{-1}]
(Latitude	27–58°N)
Reduced gravity	$g_{12}' = 1.9$, $g_{23}' = 0.96$ [10^{-2} $\text{m}^{-1}\text{s}^{-2}$]
Lateral friction	$A_H = 1.0$ [10^2 $\text{m}^{-2}\text{s}^{-1}$]
Interfacial friction	$r = 1.0$ [10^{-7} s^{-1}]

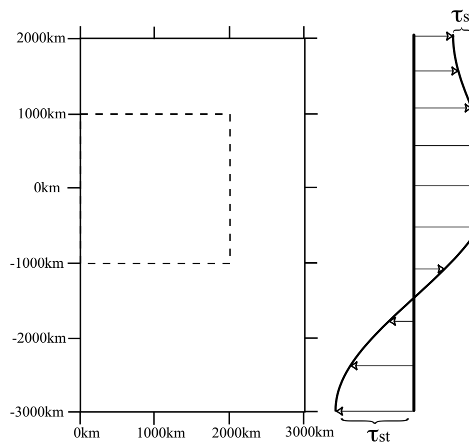

Fig. 2. Model domain and the profile of wind stress. The boundary region of two gyres, the area of our main interest and that of high resolution, is surrounded by dashed lines.

2. Numerical Model

A 2.5-layer primitive equation model is designed for this study. The governing equations for the first layer are

$$\frac{\partial u_1}{\partial t} + u_1 \frac{\partial u_1}{\partial x} + v_1 \frac{\partial u_1}{\partial y} - f v_1 = -\frac{1}{\rho_1}\frac{\partial p_1}{\partial x} - r(u_1 - u_2) + A_H\left(\frac{\partial^2 u_1}{\partial x^2} + \frac{\partial^2 u_1}{\partial y^2}\right) + \frac{\tau_x}{h_1}, \quad (1)$$

$$\frac{\partial v_1}{\partial t} + u_1 \frac{\partial v_1}{\partial x} + v_1 \frac{\partial v_1}{\partial y} + f u_1 = -\frac{1}{\rho_1}\frac{\partial p_1}{\partial y} - r(v_1 - v_2) + A_H\left(\frac{\partial^2 v_1}{\partial x^2} + \frac{\partial^2 v_1}{\partial y^2}\right) + \frac{\tau_y}{h_1}, \quad (2)$$

$$\frac{\partial p_1}{\partial z} = -\rho_1 g, \quad (3)$$

$$\frac{\partial h_1}{\partial t} + u_1 \frac{\partial h_1}{\partial x} + v_1 \frac{\partial h_1}{\partial y} = 0, \quad (4)$$

and those of the second layer are

$$\frac{\partial u_2}{\partial t} + u_2 \frac{\partial u_2}{\partial x} + v_2 \frac{\partial u_2}{\partial y} - f v_2 = -\frac{1}{\rho_2}\frac{\partial p_2}{\partial x} - r(u_2 - u_1) - r u_2 + A_H\left(\frac{\partial^2 u_2}{\partial x^2} + \frac{\partial^2 u_2}{\partial y^2}\right), \quad (5)$$

$$\frac{\partial v_2}{\partial t} + u_2 \frac{\partial v_2}{\partial x} + v_2 \frac{\partial v_2}{\partial y} + f u_2 = -\frac{1}{\rho_2}\frac{\partial p_2}{\partial y} - r(v_2 - v_1) - r v_2 + A_H\left(\frac{\partial^2 v_2}{\partial x^2} + \frac{\partial^2 v_2}{\partial y^2}\right), \quad (6)$$

$$\frac{\partial p_2}{\partial z} = -\rho_2 g, \quad (7)$$

$$\frac{\partial h_2}{\partial t} + u_2 \frac{\partial h_2}{\partial x} + v_2 \frac{\partial h_2}{\partial y} = 0, \quad (8)$$

where r is an interfacial friction coefficient. Note that there is no flow in the third layer. The model ocean has a

3000 km (zonal; 0 km ≤ x ≤ 3000 km) × 5000 km (meridional; –3000 km ≤ y ≤ 2000 km, corresponding to the latitude of 27°N to 58°N) rectangular basin (Table 1), and is driven by the wind stress in the form,

$$\tau = \begin{cases} -\tau_{st}\cos\left(\pi\left(y+3000\right)/3000\right) & \left(y \le 0\ \text{km}\right) \\ \tau_{st} + \tau_{sa}\left(\cos\left(\pi y/2000\right)-1\right) & \left(y \ge 0\ \text{km}\right), \end{cases} \tag{9}$$

where τ_{st} and τ_{sa} denote the wind stress amplitude of the subtropical and subarctic gyre. The zonally averaged wind stresses of the North Pacific are referred and idealized to be zonally homogeneous for this formulation (Table 1): in the view of the wind stress curl, there is a subtropical gyre in the southern 3000 km and a subarctic gyre in the northern 2000 km. The basic thicknesses of the layers are also simplified to be horizontally homogeneous, and their values are given so that western boundary currents could flow mainly in the first layer (hereafter referred as the upper layer), and the lower bounds of the second layer (hereafter referred as the lower layer) could be consistent with the lower bounds of wind-driven flows in the real ocean. The reduced gravity between i-th and j-th layers is

$$g_{ij}{}' = \frac{\Delta\rho_{ij}}{\rho_i} g, \tag{10}$$

where $\Delta\rho_{ij}$ is the density difference between the layers. $g_{12}{}'$ and $g_{23}{}'$ are determined considering potential density structure and the phase speed of long baroclinic Rossby waves observed in the real ocean (Chelton and Schlax, 1996). Grid spacings are 10–40 km with the high resolution of 10 km at the boundary region of the two gyres, as shown in Fig. 2. Coastal and bottom topogra-

Table 2. Experiments.

Case	τ_{st} [10^{-4} m^{-2}s^{-1}]	τ_{sa} [10^{-4} m^{-2}s^{-1}]
A (normal wind)	2.0	0.5
B (strong wind)	3.0	0.5
C (weak wind)	1.0	0.5

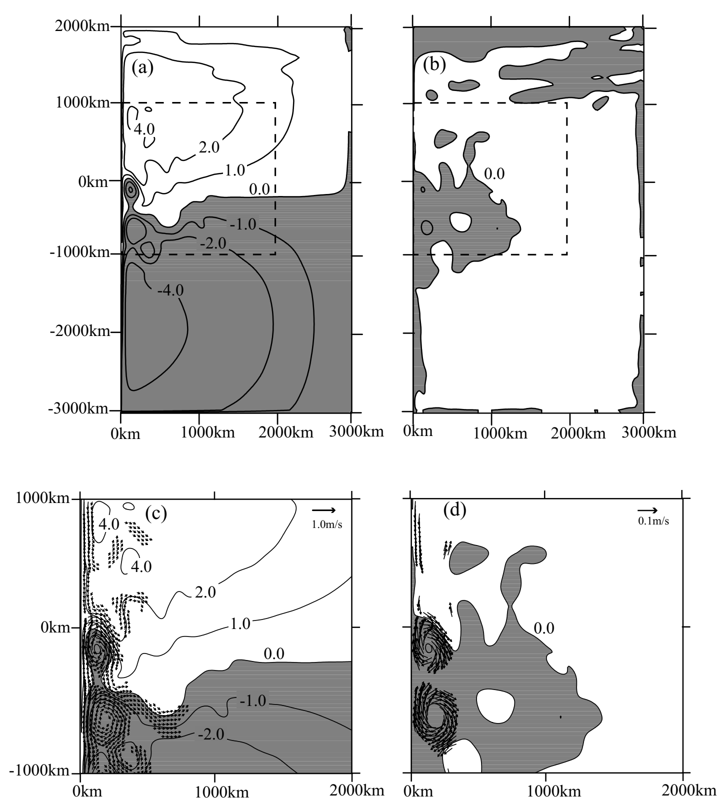

Fig. 3. Initial conditions of experiments. (a) Stream function of the first (upper) layer, (b) same as (a) but for the second (lower) layer, (c) upper layer stream function and velocity vector of the boundary region, and (d) same as (c) but for the lower layer. Contour levels are –8.0, –4.0, –2.0, –1.0, 0.0, 1.0, 2.0, 4.0, 8.0 [10^4 m^{2}s^{-2}]. The shaded areas are those where stream functions have negative values, and the boundary region is surrounded by dashed lines.

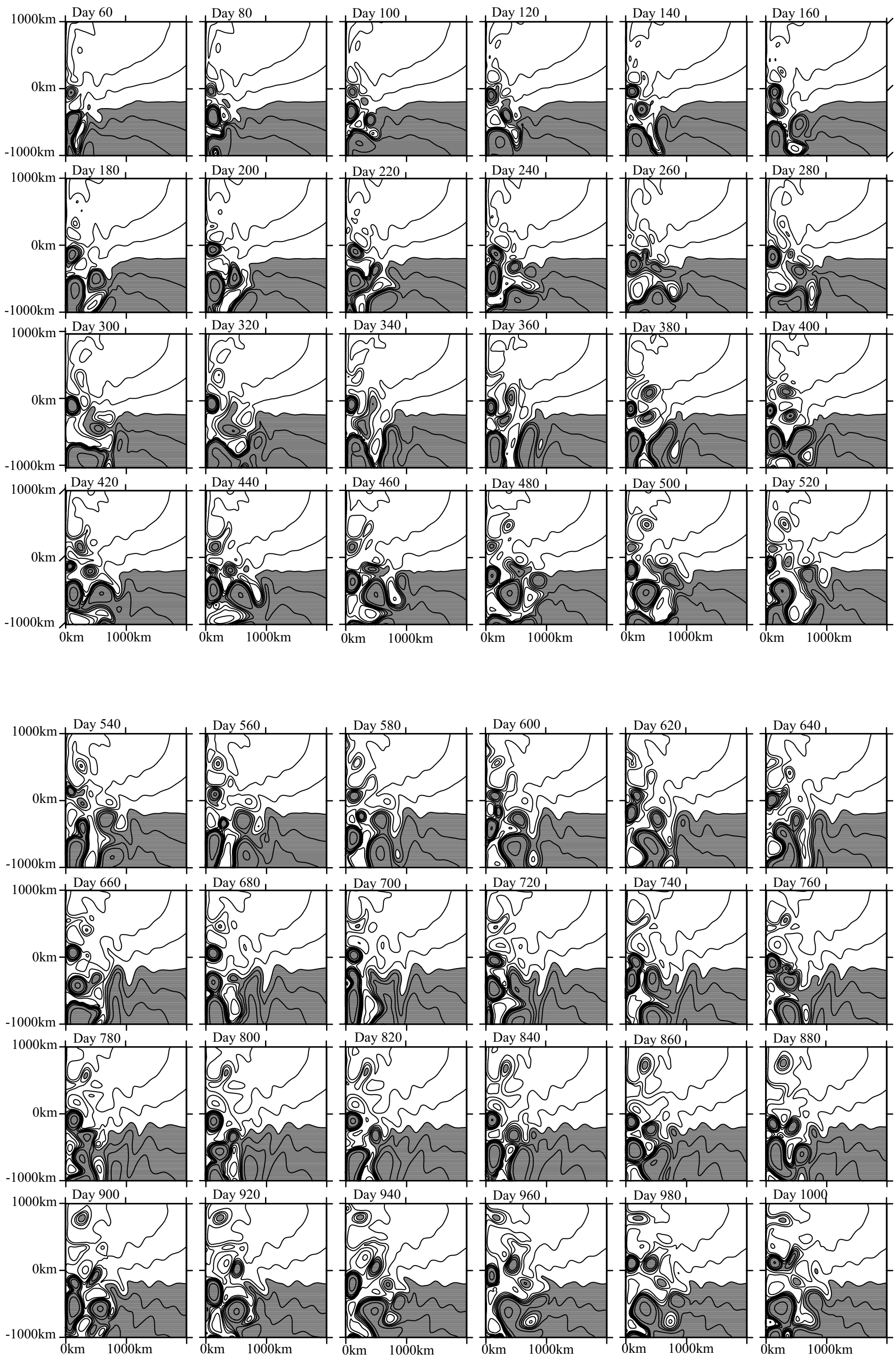

(a)

Fig. 4. Upper layer stream function of the boundary region for cases (a) A, (b) B, and (c) C. Contour levels are –8.0, –4.0, –2.0, –1.0, 0.0, 1.0, 2.0, 4.0, 8.0 [10^4 m^2s^{-2}], and the shaded areas are those where stream functions have negative values.

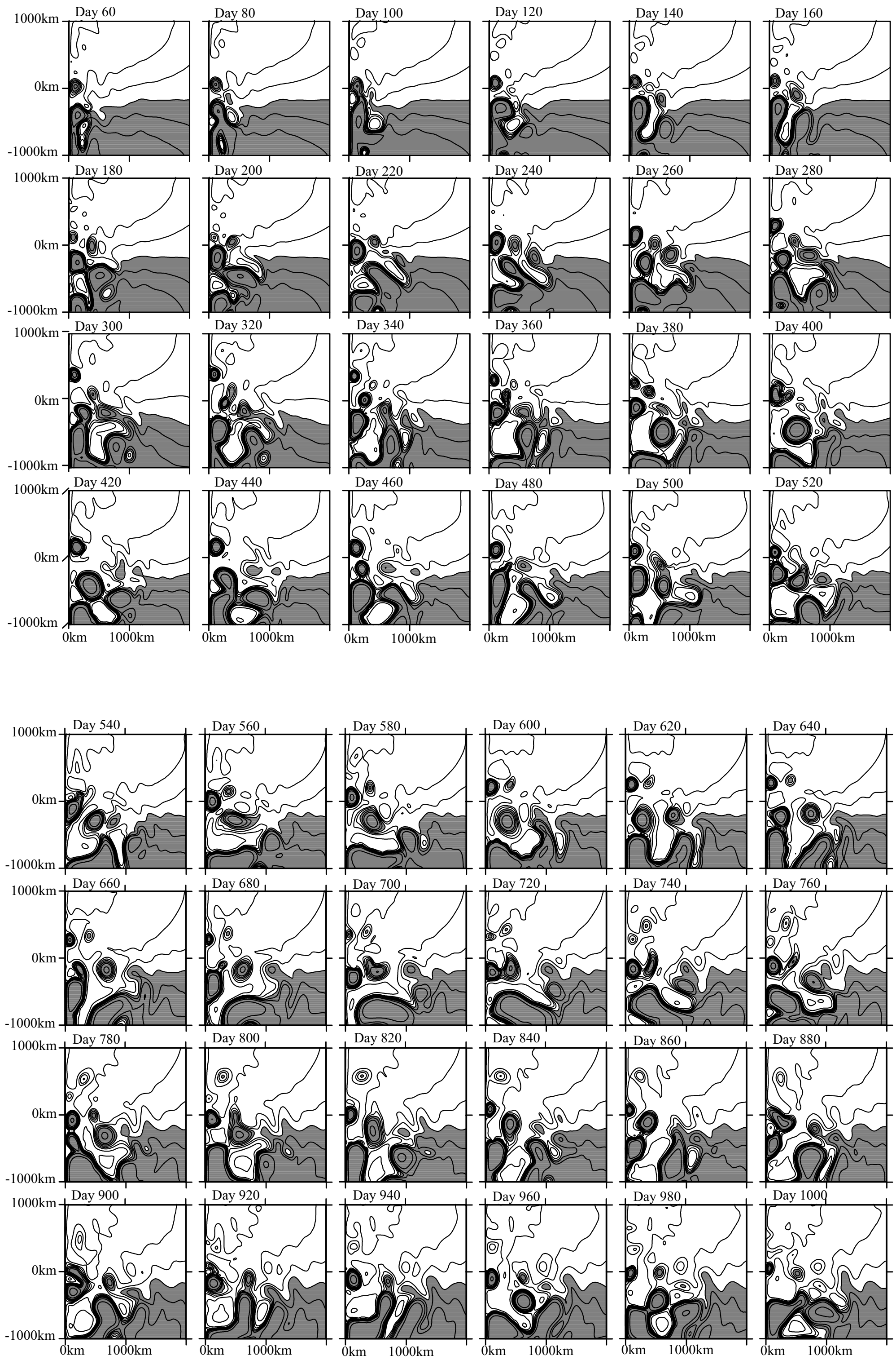

(b)

Fig. 4. (continued).

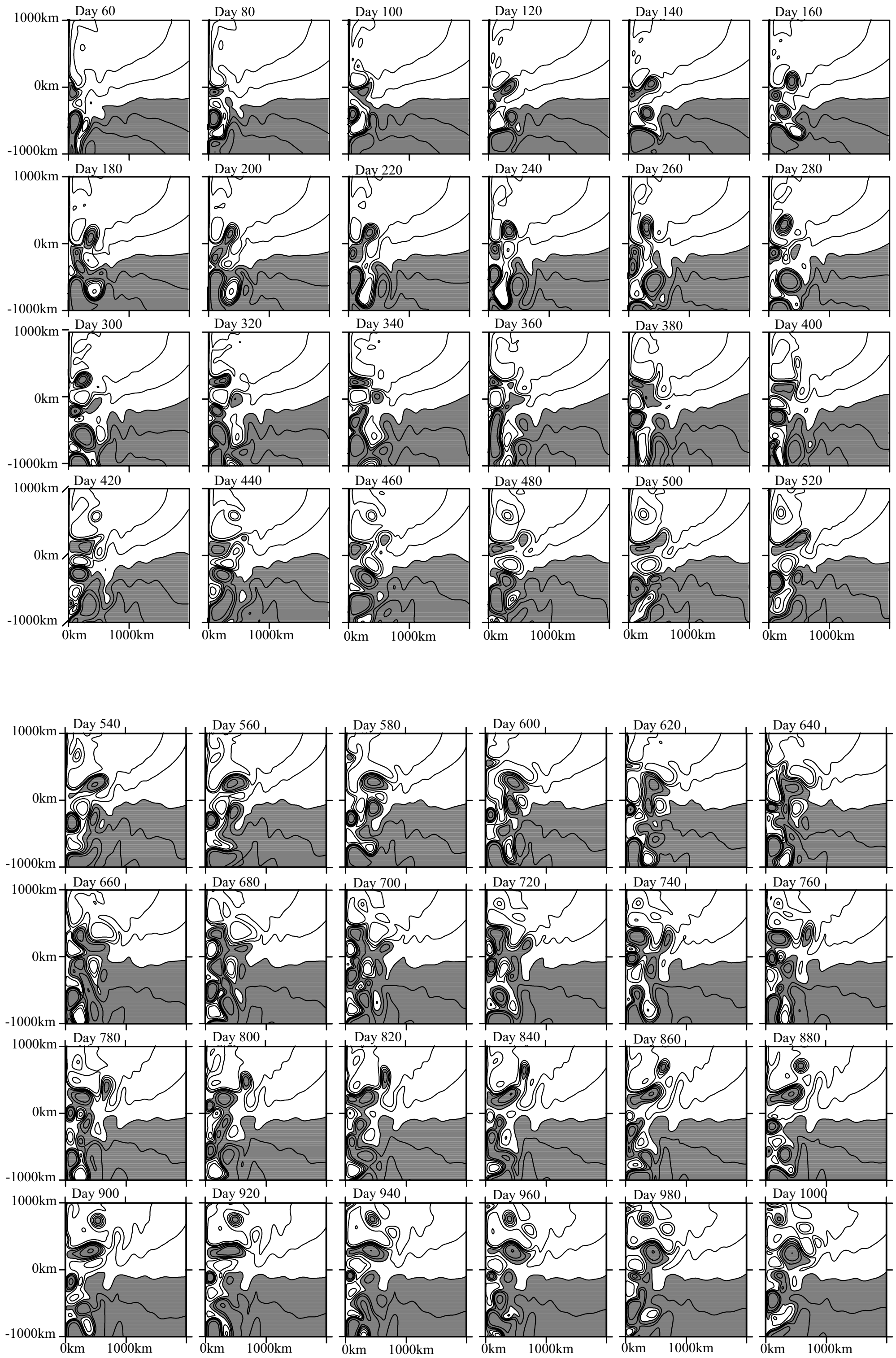

(c)

Fig. 4. (continued).

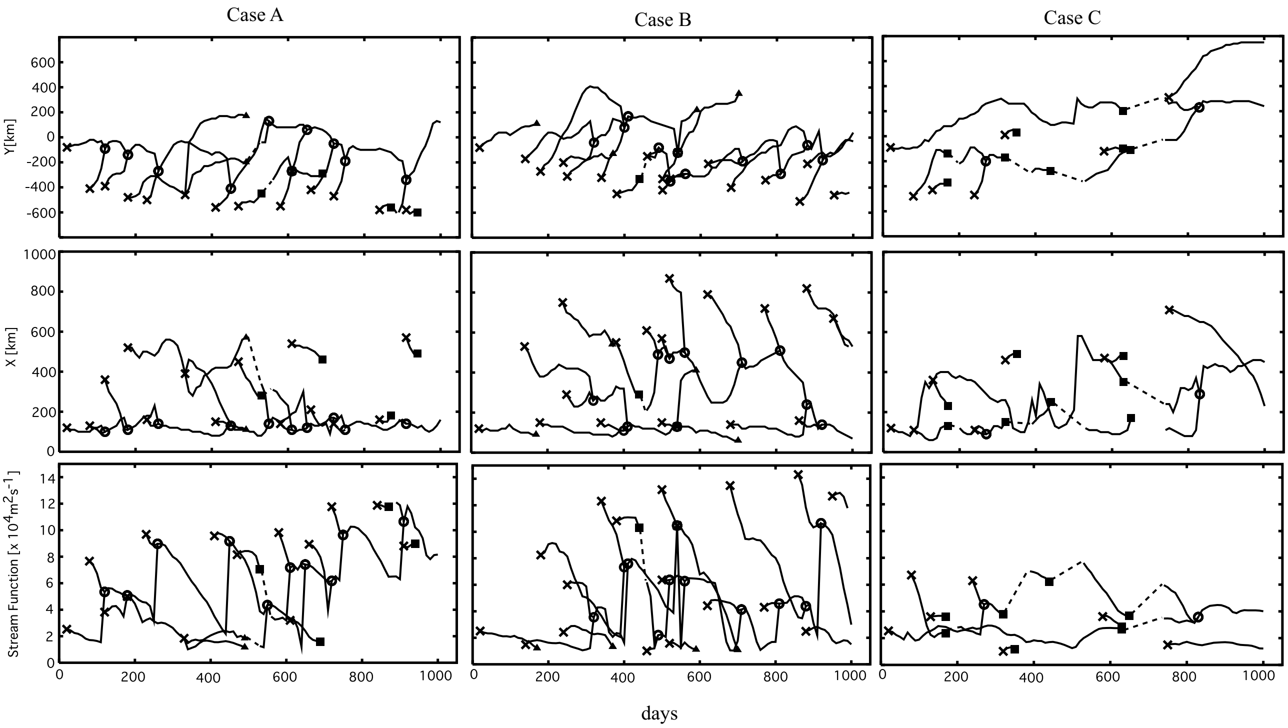

Fig. 5. Movement and intensity diagrams of warm-core rings in the mode. Rows show meridional location, zonal location, and stream function maximum, while columns correspond to cases A, B, and C. Crosses, circles, triangles, and squares indicate the formation, merging, decay, and absorption into the subtropical front, respectively. Dashed lines are drawn for periods of temporal absorption or decay to identify restored rings with previous ones.

phy is not considered for simplicity, and the no-slip condition is selected for lateral boundaries.

Warm-core rings in KOTR are generated from the Kuroshio Extension, a northern jet of a subtropical gyre mainly driven by wind forcing. We examine three cases of different wind stresses in the subtropical gyre (Table 2). In the basic case A, the maximum Sverdrup transports are about 26 Sv and 15 Sv for the subtropical and subarctic gyre, respectively; it models a double gyre system of which the subtropical one is dominant. Cases B and C are sensitivity experiments. Wind stresses are set to be constant in time for simplicity. The model domain is first spun up by the normal wind (Table 2) for 6000 days, and then daily data are averaged for 1000 days to give the initial condition of the experimental cases. The initial velocity field is presented in Fig. 3. The stream function is calculated from layer thicknesses as,

$$\psi_1 = -\frac{g}{f}\eta = \frac{g_{12}{}'}{f} z_1{}' \tag{11}$$

$$\psi_2 = \psi_1 - \frac{g_{23}{}'}{f} z_2{}', \tag{12}$$

where $z_i{}'$ denotes the displacement of the i-th layer interface from the basic state. As stream functions also well represent the instantaneous velocity field (not shown), we use them for monitoring the field in the following section. A 1000-days calculation is performed for each case.

3. Results

Figure 4 presents stream functions of the boundary region of the three cases for every period of 20 days. The northern current of the subtropical gyre following the western boundary current, corresponding to the Kuroshio Extension, flows at a few hundreds of kilometers south of the zero wind stress curl line (hereafter referred as ZWCL), as does KOTR. However, the separation point of a boundary current from a western boundary is said to depend closely on the side boundary conditions (Haidvogel *et al*., 1992). The side boundary conditions are discussed in Section 4. Rings, eddies, frontal disturbances and their interactions also appear as in the real ocean. In case A, the basic case, warm-core rings are often detached from a near-shore crest of the front (e.g. Day 60–80; as in Kawamura *et al*., 1986), move slightly northward (e.g. Day 100–140; Yasuda *et al*., 1992; Mishra and Sugimoto, 2000), are influenced by frontal disturbances

Table 3. Number of events in each case.

	Case A	Case B	Case C
Generation	14	18	7
Merging	10	11	2
Decay	2	4	0
Absorption	4	1	8

from either south or east (e.g. Day 260; Saitoh *et al.*, 1986; Yasuda *et al.*, 1992), and are blocked by the subarctic western boundary current and/or cold-core rings (hereafter referred to as subarctic flows; e.g. Day 820–860; Itoh and Sugimoto, 2001a) when they approach near ZWCL. In case B, the northern recirculation of the subtropical gyre is intensified by a strong wind, and larger, stronger rings are generated one after another. The blocking effect by subarctic flows does not clearly appear in the model, and rings go further northward along the western boundary than in case A. On the other hand, intense rings are not clearly observed as in case C. Frontal activity is moderate, and subtropical water tends to spread to the north (e.g. Day 600–700) rather than clearly detach warm-core rings. As warm-core rings (or subtropical water) go northward, the interaction with subarctic flows increases, and they tend to be advected off-shore (e.g. Day 760–800). In consequence, some rings reach the very inside the subarctic gyre (e.g. Day 860–1000) in spite of a weak wind. It should be noted that case C is important as many cold-core ring detachments occur due to the active interaction with subtropical water (e.g. Day 340).

Movement and intensity diagrams of warm-core rings for every 10 days in the boundary region are presented in Fig. 5. We track the rings in the boundary region (Fig. 2), those for which the 1×10^4 m^{2}s^{-1} contour of stream function is closed; however, this criterion is relaxed for those on the interaction with other rings or shear flows. Figure 5 shows the characteristics of the behavior of the warm-core rings in each case more clearly: northward alongshore movement of rings near ZWCL, westward movement of off-shore rings, energy supply by merging processes, and off-shore paths for a northward moving ring in Case C. The number of events (generation, merging, decay, absorption into the subtropical front following the western boundary current) are presented in Table 3. The stronger the wind stresses are, the more rings are generated, merged with other rings, and decay out, while the less they are absorbed into the subtropical front.

4. Discussion and Conclusions

Our simple model reproduces the basic processes of the warm-core rings in KOTR, and their general behavior is presented considering the difference of wind stresses.

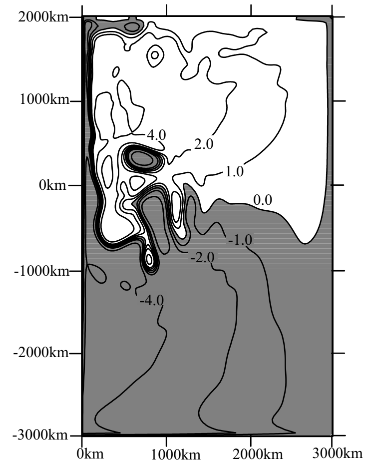

Fig. 6. Upper layer stream function of the experiment performed with free-slip condition for 1000 days. Contour levels are –8.0, –4.0, –2.0, –1.0, 0.0, 1.0, 2.0, 4.0, 8.0 [10^4 m^{2}s^{-2}], and the shaded areas are those where stream functions have negative values.

However, some simplified parameters need further discussion. The free-slip condition for lateral boundaries gives distinct descriptions from that of the no-slip condition: in the free-slip case, the western boundary current of the subtropical gyre overshoots to penetrate the subarctic gyre (Fig. 6). This pattern also appears in the quasi-geostrophic model experiments of Yasuda and Hanawa (1996). As no such penetration is observed in the counterpart, the Kuroshio Extension, we have adopted the no-slip condition for our experimental cases. Setting a vertical wall as a western boundary is to some extent justified by the steep bottom slope of the west-side of the Japan trench, off the east coast of Japan: its gradient is about 50 m km^{-1}, while the vertical/horizontal scale ratio of the typical rings is 5–20 m km^{-1} assuming vertical and horizontal scales to be 1000–2000 m and 100–200 km, respectively. Itoh and Sugimoto (2001b) suggested that the steep slope of this region behaves like a wall and rings move northward by the effect equivalent to the image effect.

The intensity of wind stresses has a direct influence on the formation of warm-core rings. South of ZWCL, a strong wind causes the detachment of intense warm-core rings, while the rings formed by a weak wind are moderate and sometimes do not clearly separate. However, the warm-core rings, either completely detached or not, move to the north near ZWCL, when interaction with subarctic flows is active. Intensified rings move northward along the coast pushing subarctic flows away. Moderate rings do not, however, and some of them are advected northeastward by the subarctic flows. In KOTR, the

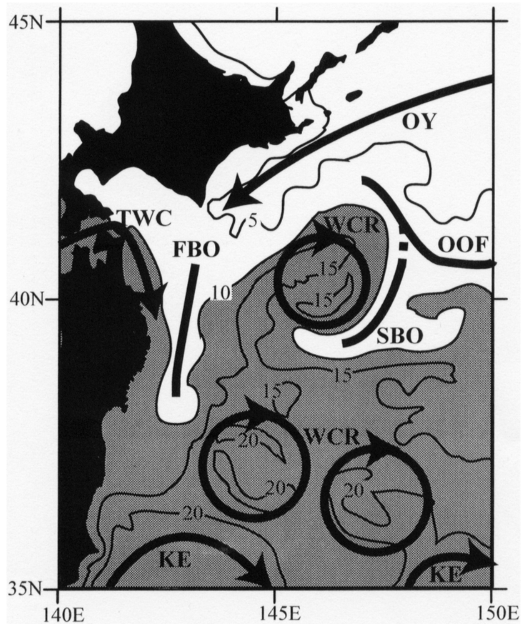

Fig. 7. Schematic illustration of the oceanic condition of KOTR over the typical sea surface temperature (SST) profile (April 1993): KE, OY, TWC, WCR, FBO, SBO, and OOF denote the Kuroshio Extension, Oyashio, Tsugaru warm current, warm-core ring, first branch of the Oyashio, second branch of the Oyashio, and off-shore Oyashio front, respectively.

subarctic western boundary current of the Oyashio intrudes with a twig-like path, and a warm-core ring is sometimes observed between the two Oyashio intrusions, which move northeastward (Fig. 7). It seems that the northeastward displacement of the moderate rings in the experiments coincides with the observation. Therefore, it is suggested that the northeastward movement of the rings between the Oyashio intrusions is due to the advection of the Oyashio.

The distribution of the Oyashio water and warm-core rings is critical in Pacific saury (*Cololabis saira*) fishing ground formation. In the North Pacific, saury migrates southward along the Oyashio water, especially along the first branch of the Oyashio (equivalent to the coastal intrusion of the Oyashio, hereafter FBO; Fig. 7) in autumn. Saitoh *et al*. (1986) analyzed satellite infrared images and suggested that the interaction of warm-core rings with the intrusions of the Oyashio such as FBO and the Tsugaru warm current controls the fishing ground formation (Fig. 7 and their figure 13). Yasuda and Watanabe (1994) presented a close relationship between the fishing ground and the large-scale oceanographic condition in the Oyashio area. They suggested that the off-shore Oyashio front (referred to be the 6°C contour line at 100 m depth from 146°E to 155°E) shifts to the north (south) when the southward extension of FBO was intense (weak), and the fishing grounds are formed relatively near-shore (off-shore). Combining these previous observations with the results of our experiments, it implies that large-scale atmospheric forcing gives important influence on the meso-scale fishing ground formation. When wind in the subtropical region is strong many strong warm-core rings are generated, and FBO is blocked or bypasses the rings and moves further south, thus contributing to the formation of fishing grounds at the north or off-shore of the ring.

Acknowledgements

We greatly thank to Dr. Crawford for his useful advices and encouragement. Thanks are extended to Dr. Shingo Kimura and the members of Fisheries Environmental Oceanography Group, Ocean Research Institute, the Univ. of Tokyo, for their useful discussion. National Space Development Agency of Japan (NASDA) and Remote Sensing Technology Center of Japan (RESTEC) are kindly acknowledged for providing SST data.

References

Chelton, D. B. and M. G. Schlax (1996): Global observation of oceanic Rossby waves. *Science*, **272**, 234–238.

Haidvogel, D. B., J. C. McWilliams and P. R. Gent (1992): Boundary current separation in a quasigeostrophic, eddy-resolving ocean circulation model. *J. Phys. Oceanogr.*, **22**, 882–902.

Itoh, S. and T. Sugimoto (2001a): Dynamics of long-term northward movement of warm-core rings and their effect on fishing ground formation. *Bull. Japan Soc. Fish. Oceanogr.*, **65**, 15–21 (in Japanese with English abstract).

Itoh, S. and T. Sugimoto (2001b): Numerical experimens on the movements of a warm-core ring with the bottom slope of a western boundary. *J. Geophys. Res.*, **106**, 26,851–26,862.

Kawamura, H., K. Mizuno and Y. Toba (1986): Formation process of a warm-core ring in the Kurohsio-Oyashio frontal zone—December 1981–October 1982. *Deep-Sea Res.*, **s11/12**, 1617–1640.

Mishra, P. and T. Sugimoto (2000): Formation processes and associated events in the evolution of Kuroshio warm core ring. *Proceedings of the PORSEC 2000 Goa, India*, Vol. 2, 565–570.

Mizuno, K. and W. B. White (1983): Annual and interannual variability in the Kuroshio Current System. *J. Phys. Oceanogr.*, **13**, 154–159.

Saitoh, S.-i., S. Kosaka and J. Iisaka (1986): Satellite infrared observations of Kuroshio warm-core rings and their application to study of Pacific saury migration. *Deep-Sea Res.*, **s11/12**, 1601–1615.

Verron, J. and L. Provost (1991): Response of eddy-resolved general circulation numerical models to asymmetrical wind forcing. *Dyn. Atmos. Oceans*, **15**, 505–533.

Yasuda, I. and Y. Watanabe (1994): On the relationship between the Oyashio front and saury fishing grounds. *Fish. Oceanogr.*, **3**, 172–182.

Yasuda, I., K. Okuda and M. Hirai (1992): Evolution of a Kuroshio warm-core ring—variability of the hydrographic structure. *Deep-Sea Res*., **39**, S131–S161.

Yasuda, T. and K. Hanawa (1996): Influence of asymmetric wind stress curl on the general ocean circulation using an eddy-resolbing quasi-geostrophic model. *J. Oceanogr*., **52**, 189–206.